Journal of Sol-Gel Science and Technology
https://doi.org/10.1007/s10971-023-06193-9

ORIGINAL PAPER

Preliminary study on the design of superhydrophobic surface by 3D inkjet printing of a sol-gel solution

Rosa Taurino[1,2] · Maria Cannio[3] · Dino Norberto Boccaccini[3] · Massimo Messori[2,4] · Federica Bondioli[2,4]

Received: 17 May 2023 / Accepted: 19 July 2023
© The Author(s), under exclusive licence to Springer Science+Business Media, LLC, part of Springer Nature 2023

Abstract

In this study a novel and straightforward 3D printing method based on inkjet printing process for the design of superhydrophobic surfaces was investigated. In particular, a novel sol-gel solution was designed and used with a modified 3D printing approach based on micro-solenoid inkjet printing. The study focuses on the impact of roughness and chemical composition - both crucial factors in achieving superhydrophobic properties - by measuring the contact. In addition, tilt angle of water droplets on different coating were determined. It is believed that the simple new inkjet printing method presented here can expand the application of the superhydrophobic high and low adhesive surface on different substrates for application in many industrial fields.

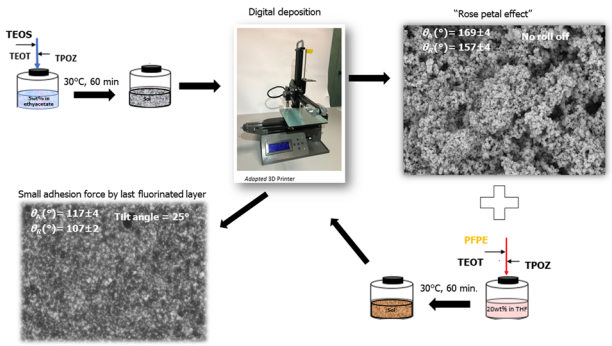

Keywords Inkjet printing · Superhydrophobic surfaces · Sol–gel process · Water repellence.

1 Introduction

The development of superhydrophobic surfaces (SH), characterized by a water contact angle higher than 150° and low surface energy, have been researched and for a long time by academia and industry [1]. Moreover, it is now well established that to achieve a superhydrophobic surface, it is necessary to combine these coatings, characterised by low surface energy, with a hierarchical surface structure [2]. In particular, the surface structuring/architecture favours the air gaps between the water drop and the surface, which a further decrease in adhesion. In this way, coatings with hydrophobic properties applied to structured surfaces at two different length scales (microstructure and nanostructure)

✉ Rosa Taurino
rosa.taurino@unifi.it

[1] Department of Industrial Engineering, University of Florence, Via di Santa Marta 3, Firenze 50139, Italy

[2] National Interuniversity Consortium of Materials Science and Technology (INSTM), Via Giusti 9, Firenze 50121, Italy

[3] Resoh Solutions SRL, Via Pietro Giardini 476/N, 41124 Modena, Italy

[4] Department of Applied Science and Technology, Politecnico di Torino, Corso Duca Degli Abruzzi 24, Torino 10129, Italy

Published online: 27 July 2023

reduce the interaction between water and surface, affecting the liquid drop to not penetrate the grooves on the surface structure in a state that is referred to as Cassie-Baxter or "fakir-bed" [3, 4]. In this condition, water droplets roll-off from the surfaces when they are tilted by even a few degrees, as is also the case with the lotus leaf (lotus effect). Nowadays, superhydrophobic structures can find applications to avoid snow sticking, biofilm formation, contamination, corrosion, separate oil and water, guarantee self-cleaning, increasing buoyancy and reducing resistance in microfluidic systems [5].

Several methods have been reported on the development of superhydropobic rough films [6–10], boehmite rough surface is formed by the sublimation of aluminum acetylacetone [7], anodic oxidation of aluminum and subsequent coating by a low surface energy [9], the chemical vapor deposition of fluoroalkylsilanes, radio frequeancy plasma ething followed by fluorodecyltrichlorosilane coating are able to create a superhydrobhobic surfaces with controlled roughness [10]. On the other hand, there are several deposition techniques, examples of which are electrospinning [11], sol-gel process or chemical vapor deposition [12].

The sol-gel method can be a very efficient approach for low cost, fast and flexible production of self-cleaning coatings with structured surface [6]. For example, the deposition of mixtures of several liquid metal alkoxides $M(OR)_x$ by spray-coating followed by a last α,ω-trialkoxysilane-terminated PFPE, was able to create superhydrophobic coatings with two different length scales [6]. This is an example of process in that layer-by-layer deposition solution by spray coating led to achieving random rough surfaces with water repellent wetting behaviour. New approach for the deposition of thin films is the 3D printing process. Recently, different additive manufacturing (AM) techniques have attracted much interest for the deposition of thin films. Many examples of coatings based on 3D printing approach are given in literature [13, 14]. According to Wang et al. [15], the utilization of vinyl-terminated monomers and chemically modified surfaces in 3D printing can lead to a transformation of surface properties, transitioning them from hydrophilic to superhydrophobic.

Zhang et al. [16] used digital ultraviolet litography to print a solution that contained a dispersion of polytetrafluoroethylene (PTFE) nanoparticles in a photocurable solution. Li et al. [17] investigated the advancement of an affordable "multi-scale stereolithography" approach for fabricating objects at macroscale level with microscale surface architectures. This study demonstrated the potential to apply 3D printing approach as a powerful tool that can bring bioinspired structures into real-life applications. Han et al. used 3D-printing technology to create biomimetic hybrid (hydrophilic/hydrophobic) surfaces for water harvesting. They used multiple processes to rapidly and simply fabricate nano/micro-roughness surfaces with water contact angle of 136° for various application [18].

Herein, we report a preliminary study on the 3D printing fabrication of SH surfaces using sol-gel process and inkjet printing technique. The sol-gel process could be a potentially interesting method to produce SH surfaces by inkjet 3D printing technology. In fact, 3D inkjet printing process proceeds through layer-by-layer deposition similar to other 3D printing process, providing an easy method to create films with surface structure which can help to increase superhydrophobic films productivity. SH surfaces fabrication using a sol-gel approach is currently not widely implemented in large-scale manufacturing. Even then, the implementation of sol-gel technique in combination with 3D inkjet printing technology offers important advantages. Infact, the high precision of dispensing solution volume, as well as the high precision in the solution localization during the injection process onto the surface provides a more efficient way to deposit the precursor solution reducing the solution consumption. Moreover, careful control of solution parameters (solution composition and reological properties), as well as environmental condition (temperature, etc,) can avoid, for example, the splashing phenomena [19–22]. The viscosity and density of the solution are crucial parameters for achieving optimal printing performance. Additionally, surface tension plays a vital role in forming uniform and well-defined droplet shapes during the printing process [23]. Thus, the increasing demand for the customized production of superhydrophobic (SH) films has led to the exploration of 3D inkjet printing as an appealing method for fabricating structured surfaces on diverse substrates. In this work, solenoid valve inkjet printing was selected for the application of sol-gel solutions carefully optimized in terms of viscosity, surface tension and density. After the digital deposition, the impact of chemical composition and final microstructure on the coating hydrophobic properties were studied. In particular, the wetting behaviour, being dependant on topology and morphology of surfaces, contact angle hysteresis (CAH) and roll-off angle are studied to predict the probability of achieving superhydrophobic properties. To assess the impact of roughness on wettability properties, it is necessary to measure advancing and receding contact angles (CAs). This helps determine whether the structure exhibits the "Lotus effect" (high CAs and low CA hysteresis) or the "Rose petal effect" (high CAs and high CA hysteresis), thus providing insights into the development of the surface structure [24].

2 Experimental section

2.1 Materials

The chemicals employed in the preparation of films are silane-terminated PFPE (named FLKS10, purchased from Solvay-Solexis), Tetrahydrofuran (THF, Carlo Erba) and ethyl acetate (Carlo Erba). The inorganic sol was synthesized from the silica precursor using tetraethyl orthosilicate (TEOS, Sigma–Aldrich >99.9%), tetraethyl orthotitanate (TEOT, Sigma–Aldrich >95%) was used as titania precursor and tetra-n-propyl zirconate (TPOZ, Sigma–Aldrich >99%) was used as zirconia precursor. In a typical experiment, the sample TZS was prepared by the deposition onto glass substrate of solution mixture of TEOT/TPOZ/TEOS dissolved in ethyl acetate at a concentration of about 5 wt.% under stirring for 10 min. As reported in a previous work [6], the final weight ratio of titania (TiO_2), zirconia (ZrO_2) and silica (SiO_2) was 25:36:39 wt% respectively. The sol was prepared by gradually mixing TEOS and ethyl acetate solvent. After stirring for 5 s, TEOT was added to the TEOS sol while continuing to stir. After 10 s of homogenization, TPOZ was added. The resulting mixture was stirred for 10 min at room temperature (approximately 22 °C) and a relative humidity (RH) of 45–50%. To achieve the desired viscosity for micro-solenoid inkjet 3D printing technology, the sol-gel compositions underwent prehydrolysis before deposition to enhance solution performance. Initially, the sol-gel solutions were applied to substrates immediately after 10 min of stirring at room temperature, but drop splitting occurred. As a result, the solutions were placed in closed vials and placed in an air circulation oven at 30 °C for 1 h to allow partial progression of the sol-gel reaction. Figure 1 shows an image of the final TZS sol-gel solution used in the 3D inkjet fabrication process. The obtained solutions were then 3D printed onto glass plates that were polished with a standard RCA1 solution (NH_4OH:-H_2O_2:H_2O = 1:1:5). The cleaned glasses were subsequently ultrasonicated in distilled water.

The sample TZF was obtained by the deposition of a sol-gel solution of TEOT, TPOZ and FLKS10, according to a procedure developed in a previous work [6].

Finally, the bilayer sample TZS/TZF was prepared by sequential deposition of two layers so that the fluorinated organic-inorganic TZF layer was deposited to modify the chemical surface of TZS sample. All the formulations were applied by 3D inkjet processing.

2.2 Inkjet printer

The optimized sol-gel solutions were deposited using a home-made micro-solenoid inkjet 3D printing machine (see Fig. 2). The printer was built from a modified commercial

Fig. 1 Sample of optimized TZS sol-gel solution after 1 h of stirring at 30 °C

Fig. 2 Home-made micro-solenoid inkjet 3D printing machine

FDM 3D printer (Anycubic Kobra). In particular, the extruder of the 3D printer was replaced by a system consisting of a direct actuated 2-way micro-solenoid valve (type VA204-508, Staiger), having a nozzle diameter of 0.3 mm, which is fed through a hydraulic circuit from a pressurized air ink container tank. A digital pressure sensor was employed to regulate the pressure level within the tank,

while this pressure reading, in conjunction with the duty cycle supplied to the electro valve via a pulse-width modulation (PWM) control system, determined the ink discharge rate at the nozzle exit. The best conditions in homogeneity and thickness of the deposited layers were obtained at a pressure of the ink tank of about 0.4–0.6 bar. In this study, direct-acting micro-solenoid valves were utilized, which operate in a fully open or fully closed manner. To control the valves, a specially designed Pulse Width Modulation (PWM) control system was implemented. The system broke down the voltage into a series of "on" and "off" pulses, varying the duty cycle. By adjusting the amplitude or duration of the voltage pulses, the valve opening time was controlled, allowing control over the flow rate. In this work, a duty cycle of 50% at a frequency of 200 Hz was used. The PWM signal was generated using an ARDUINO UNO board and controlled through a LabVIEW program. The digital model was created using Microsoft®'s free 3D Builder software, and a parallelepiped with dimensions of $50 \times 25 \times 0.5$ mm was used as the model layer for suspension deposition. The digital model was then managed using the open-source software Slic3r, commonly employed for generating GCode files in 3D printing. The tests were performed at a temperature of 25 °C. A solid film printed on a glass substrate (standoff distance of 1250 µm) underwent condensation reactions to form metal oxide system. This involved placing the films in a 100 °C oven for 2 h to complete the reaction.

2.3 Characterization

2.3.1 Solution characterization

As reported above, the critical parameters to achieve good printing performance in inkjet printing are the viscosity value of solution, density and surface tension. Then, viscosity, surface tension, density and pH were measured for the sol-gel solutions pre-hydrolized for 1 h. The density of solutions was determined by weighing 1 mL of the solution three times using an analytical balance. The viscosity was measured using a rheometer (RheoStress RS100, HAAKE^{TM}) with a cone-plate tool (60 mm diameter, 1° angle). Then, surface tension analysis was performed by pendant drop method. In particular, by using the ADSA (Axysimmetric Drop Shape Analysis) technique and the OCA 20 apparatus (DataPhysics Instrument GmbH, Filderstadt, Germany) [25], surface tension data was obtained.

2.3.2 Coated glasses characterization

The water contact angle and sliding angle of the films were measured by using an OCA 20 apparatus from DataPhysics Instrument GmbH, Filderstadt, Germany. Prior to the measurements, the specimens were immersed in THF for 30 s to prevent surface contamination. After drying, static, dynamic contact angles were measured with distilled water. The water contact angle and sliding angle of the films were measured using an OCA 20 apparatus from DataPhysics Instrument GmbH in Filderstadt, Germany. Prior to the measurements, the specimens were immersed in THF (tetrahydrofuran) for 30 s to prevent surface contamination. After drying, static and dynamic contact angles were measured using distilled water. The final contact angle for each film was calculated by averaging 10 measurement data points from different areas. The roll-off angle was determined by tilting angle. Water droplets of 15 µl volume were placed on the samples fixed to a tilted flat plate. The plate was gradually tilted until the drop started to move. The rolling angle was determined using a scale that provided a measurement precision of approximately 0.5 degrees. At least five measurements were taken for each sample. All measurements were conducted under constant conditions, including a temperature of 25 ± 0.5 °C and relative humidity of $40 \pm 3\%$.

A morphological investigation was carried out using a SEM-FEG (Nova NanoSEM 450, FEI, Eindhoven, Netherlands) by applying a voltage of 8 kV. The micromorphological features were evaluated by optical confocal profilometry (ConScan profilometer, CSM Instruments) used also to measure the roughness parameters. For surface roughness characterization, various parameters were calculated from 500×500 µm² scale images. These parameters include the root square mean roughness profile (Rq), the maximum height of the profile (Rz), the maximum roughness height (Rt) and the waviness (Wz).

3 Results and discussion

3.1 Properties of printable solutions

To enhance the jetting stability and in particular the final viscosity for the intended application, the sol-gel solutions underwent pre-hydrolysis for a duration of 1 h. Infact, in the first step of study the sol-gel solution was applied after just 10 min of stirring and splashing phenomena was observed due to the very low viscosity solution (lower than 1 mPa*s), not compatible with the 3D jetting printing. Then, before printing process, pre-hydrolized process was necessary to drive the condensation process thus the formation of small oligomers producing viscosity increase. Table 1 shows the physico-chemical properties of the optimised solutions for digital processing after 1 h of stirring in closed vials and in an air circulation oven at a temperature of 30 °C. The surface tension and viscosity values were selected to be compatible with the used inkjet printing process [26]. Since, as

Table 1 Optimised physicochemical properties of sol-gel solutions for inkjet 3D prinitng process

	Solution TZS (1 h)	Solution TZF (1 h)
Surface tension (mN/m)	26.5	20.2
Density (g/cm^3)	0.90	0.88
Viscosity at 250 s^{-1} (mPa*s)	3.96	1.33
pH	6	6

Table 2 Wetting properties (static (θ_S), advancing (θ_A), and receding (θ_R) water Cas, CA hysteresis (CAH) and tilt angle respectively

Sample ID	θ_S (°)	θ_A (°)	θ_R (°)	CAH	tilt angle
Glass substrate	20 ± 2	n.d	n.d	n.d	n.d
TZF(1 h)	78 ± 2	80 ± 2	75 ± 1	5	30
TZS(1 h)	162 ± 4	169 ± 4	157 ± 4	12	No roll off
TZS/TZF(1 h)	112 ± 2	117 ± 4	107 ± 2	11	25

the sol-gel reaction time prolongs, precipitation reaction occurred clogging the nozzle tip, 1 h of reaction time was selected as the best condensation time before deposition process.

The different viscosity of TZF solution with respect to TZS could be ascribed to the slower rate of condensation process.

3.2 Properties of printed surfaces

3.2.1 Surface wettability

Table 2 presents a range of parameters utilized to characterize surface wetting, including static and dynamic contact angles (CAs) as well as contact angle hysteresis. The sample TZF(1 h) demonstrated static, advancing, and receding contact angles ranging from 80° to 75°. The sample TZF(1 h) possessed values of static, advancing, and receding CAs in the range of 80–75°. It is notable that this behaviour is due by the hydrophobic properties of the perfluorinated polyether film, as suggested previously for various perfluoropolyethers [27]. By comparing the wetting behaviour of the fluorinated coating TZF(1 h) and no-fluorinated TZS(1 h) sample, we can observe that TZS(1 h) had CAs 80° higher than those of TZF(1 h) thus superhydrophobic behaviour was obtained for this last one sample. In fact, it possesses an advancing and receding water CAs of 169° and 157°, respectively. In order to increase the hydrophobic chemical of TZS(1 h), the fluorinated TZF(1 h) film was deposited, using the approach already adopted in previous work [6, 24] involving the modification of inorganic fractal coatings by fluorinated based films. In contrast to earlier studies [6, 24], in this work the application of TZF(1 h) film by 3D printing approach led immediately to a decrease in the wetting behaviour of TZS(1 h) sample (Table 2). Infact, water advancing and receding CAs of the final sample TZS/TZF(1 h) were in the ranges 117°–122° and 107°–109°, respectively.

Table 3 Roughness parameters (Rq, Rz, Rt) obtained by optical confocal profilometry (Conscan profilometer, CSM Instruments)

Sample ID	Rq (μm)	Rz (μm)	Rt (μm)	Wz (μm)
Glass substrate	n.d	n.d	n.d	n.d
TZS(1 h)	4.6 ± 1.5	24.1 ± 3.8	34.8 ± 3.3	11.4 ± 6.6
TZS/TZF(1 h)	2.3 ± 1.2	12.7 ± 3.3	26.6 ± 5.6	6.9 ± 1.9

The elevated contact angle hysteresis (CAH) observed in the TZS(1 h) thin film sample, which is based on inorganic oxides, suggests the existence of regions on the surface that hinder the detachment of the contact line. Indeed, when solid surfaces possess inherent roughness or chemical heterogeneity, the contact line between the solid surface and the liquid remains fixed within a range defined by the receding and advancing contact angles. As a result, even when the inclination angle reaches 90°, the droplet remains pinned to the surface [28]. This result is confirmed by rolling angle measurements. Infact, even if the TZS(1 h) sample was tilted of 180°, no roll-off angle was measured, indicating a highly adhesive force ("Rose petal effect") [29]. After adding fluorinated layer TZF(1 h), the as obtained TZS/TZF(1 h) sample shows a tilt angle of 25° (Table 2). Therefore, even if the application of a last fluorinated layer is able to decrease the adhesive force to water liquid, it reduces the dynamic CAs thus no superhydrophobic properties was developed.

3.2.2 Surface roughness and microstructure

To better understand the wettability behaviour of the developed coatings, the sample roughness was determined by optical confocal profilometry. As reported in Table 3, a significant decrease in roughness values was noted after the application of fluorinated TZF(1 h), suggesting that the roughness depends on the chemical composition of the deposited sol-gel solutions. SEM micrographs and confocal results offered compelling evidence of a diverse array of structural textures present on the functionalized surfaces. The confocal topography of TZS(1 h) sample (Fig. 3a) shows a film with submicron particles agglomerates, while a smooth surface was observed for TZS/TZF(1 h) film. The confocal microscopy data, as shown in Table 3, revealed a noteworthy disparity in the Ra, Rq, and Wz values between the TZS(1 h) sample and the TZS/TZF(1 h) sample after the application of the fluorinated-based layer. A significant

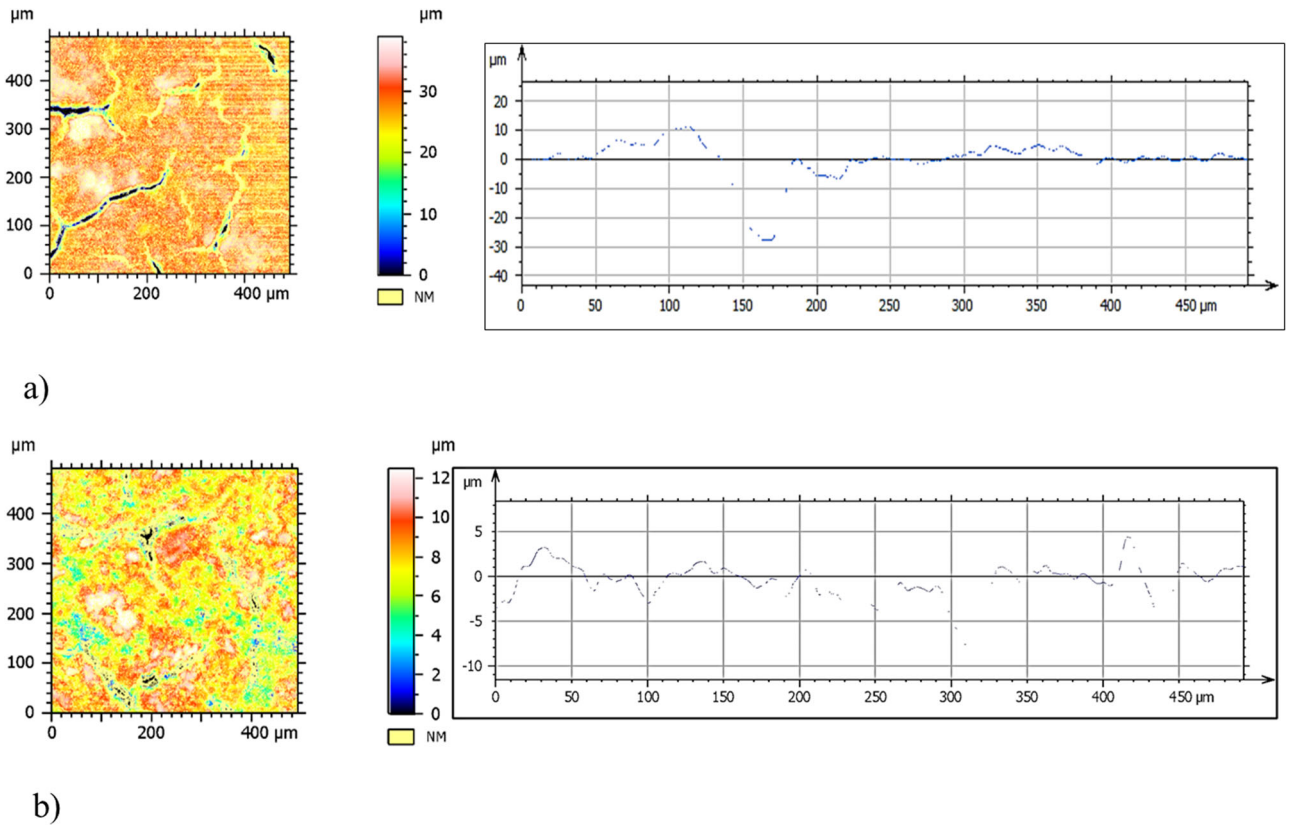

Fig. 3 Surface-topographic features and profile obtained with confocal microscopy of (**a**) TZS (1 h) and (**b**) TZS/TZF(1 h) samples

decrease in Rq and Rz values was noted. As an example, the Rq value was determined to be 4.6 µm for the TZS(1 h) film and 2.3 µm for the TZS/TZF(1 h) film. This indicates that the roughness resulting from the application of the inorganic layer is reduced by the thin fluorinated layer, which fills the surface irregularities and pores on the TZS(1 h) surface.

The results obtained from the confocal topography were also confirmed by the SEM images. Figure 4a, c show SEM images of the TZS(1 h) and TZS/TZF(1 h) samples, respectively, which were prepared by inkjet printing and subsequently thermally treated at 100 °C. At lower magnification, it can be observed that the application of the TZF(1 h) solution on the TZS(1 h) layer (Fig. 4c) resulted in a slightly rough surface compared to the texture of the TZS(1 h) sample (Fig. 4a). The presence of the fluorinated coating is clearly visible at lower magnification. At higher magnification (Fig. 4b, d), a fine texture at the nanoscale level is noticeable. The surface of the TZS(1 h) sample (Fig. 5a) is composed of microaggregates consisting of nanoparticles with dimensions ranging from 120 to 200 nm (Fig. 5b).

It is worth noting that different deposition techniques can lead to distinct structures and distributions of metal species, as indicated by previous research [6]. After the application of the fluorinated-based film, the original surface morphology of the TZS(1 h) sample underwent changes, resulting in a surface with fewer wrinkles and porosity (Fig. 3b). These observations suggest that the addition of the fluorinated coating modifies the surface properties of the TZS(1 h) sample, leading to a smoother surface compared to the original texture Fig. 6. The SEM images provide visual evidence of the morphological changes induced by the application of the TZF(1 h) solution.

4 Discussion

It is well evident that the physicochemical properties of solution represent important parameters to control the fluid performance in 3D printing. First of all, in order to obtain the appropriate viscosity for micro-solenoid inkjet 3D printing technology, the sol-gel compositions were pre-hydrolized to increase the jetting stability and to avoid the splashing phenomena. In particular, in the study to increase the viscosity of sol-gel solution before printing process, the reaction time t_r was fixed at 1 h to obtain a proper jettability and in particular a viscosity higher than 1 mPa*s. In this work the viscosity of the sol-gel solution was less than 10 mPas and higher than 0.5 mPas. The lower viscosity of the TZF(1 h) solution can be ascribed to the lower condensation reaction and then to smaller extend of oligomers.

After fine-tuning the printing parameters for super-hydrophobicity, we created multilevel structured surfaces

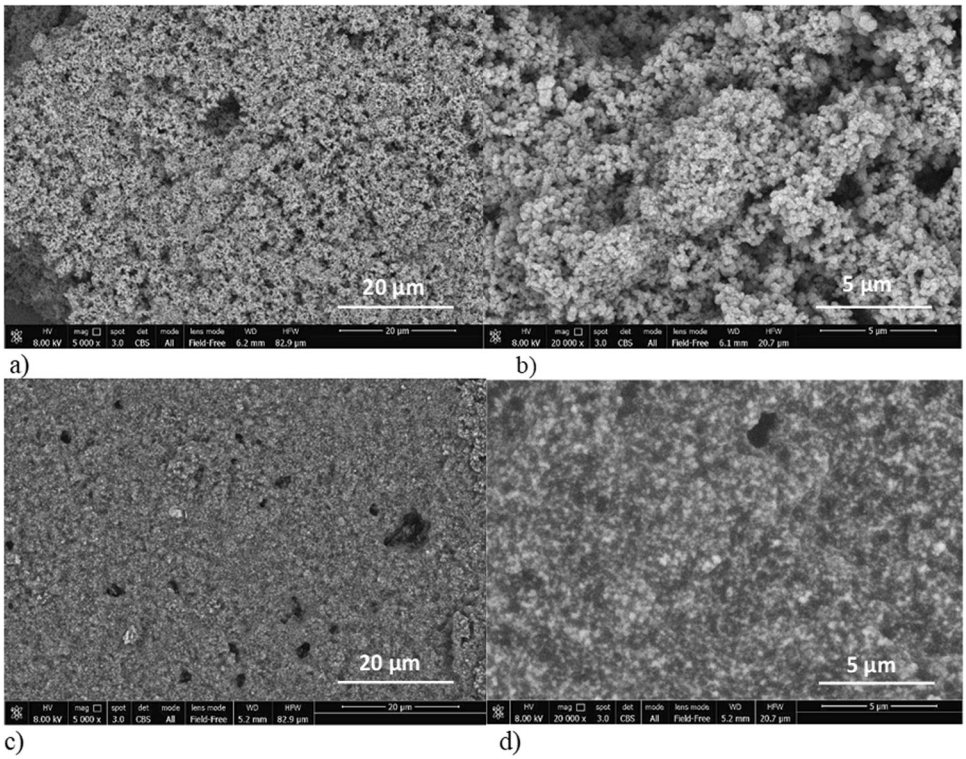

Fig. 4 SEM images of the surface (top view) of: (**a**) TZS(1 h) at 5000x; (**b**) TZS(1 h) at 20000x, (**c**) TZS/TZF(1 h) at 5000x and TZS/TZF(1 h) at 20000x

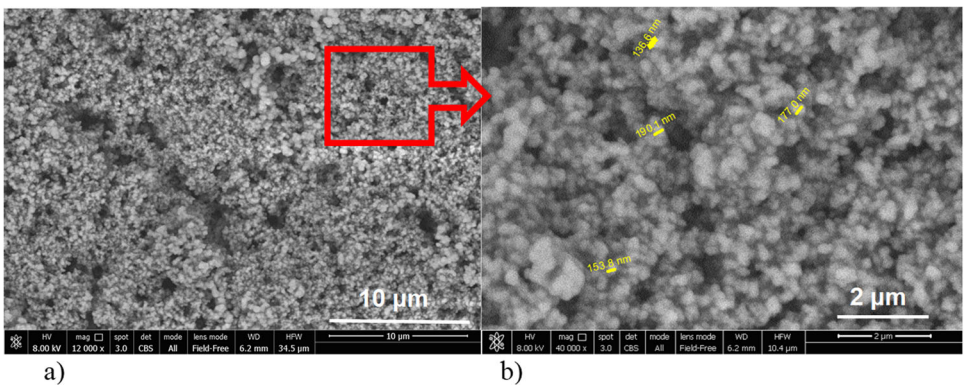

Fig. 5 SEM images of the surface (top view) of TZS(1 h) (**a**) at 12000x and (**b**) 40000x

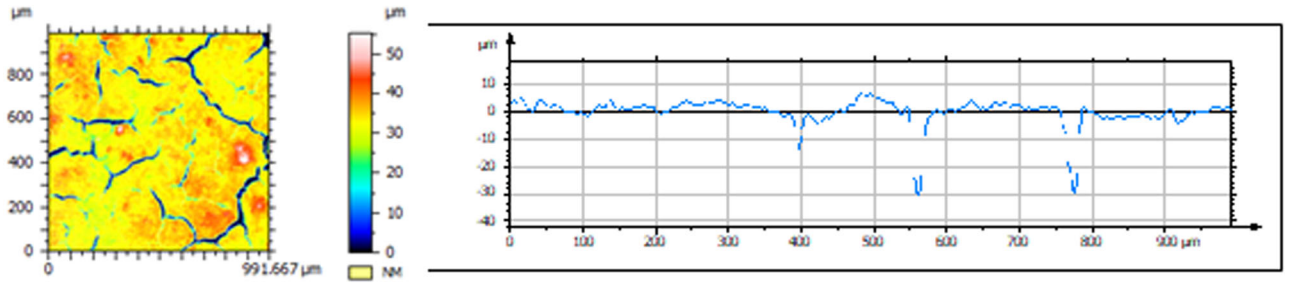

Fig. 6 Surface-topographic features and profile obtained with confocal microscopy of TZS(1b h) sample (1000 × 1000 µm² scale image)

by depositing sol-gel solutions consisting of various metal alkoxides with different reaction times. Then, the 3D inkjet printing of TZS (1 h) solution, enables the formation of complex structure with microaggregates made of nanoparticles thus a surface roughness that is critical for the final wettability. Based on the observed hierarchical micro- and nanostructures on the surface of the TZS(1 h) sample, it is reasonable to propose that the wetting behavior of the sample corresponds to the Cassie impregnating wetting state [30]. Water droplets are anticipated to enter into the larger

micron scale cavities of the coating while bypassing the smaller ones, thus, to form the Cassie impregnating wetting regime [31–33]. These findings indicate that superhydrophobicity can be achieved with a sub-micrometer level of surface roughness, as characterized by a root mean square (Rq) roughness value of 4.6 µm, along with the presence of micrometer-sized features. The peak-to-valley height roughness (Rz) is on the order of several micrometers. However, it is important to note that the sample also exhibits a high adhesive force with water, commonly known as the "Rose petal effect."

Probably a contribution to work of adhesion could be due to the presence of unreacted ethoxide groups of metal alkoxides. The presence of unreacted ethoxide groups from the metal alkoxides could potentially contribute to the work of adhesion. The adhesion force between water droplets and the sub-microstructured surface is reduced when a fluorinated layer is deposited. This decrease in adhesion force prevents the droplets from being firmly anchored when the surface is tilted at an angle of 25°. As a result, the water droplets slide down the surface rapidly.

In the case of TZS/TZF(1 h) sample, its lower adhesive property can be ascribed to the presence of hydrophobic groups of organic phases. The different texture obtained after the printing of TZF(1 h) solution could be due to the different reaction rate of sol-gel process. A higher hydrolysis rate can be supposed during the printing of the TZF(1 h) solution at environmental condition.

5 Conclusion

In this study we report a preliminary study on the design of superhydrophobic surfaces using sol-gel process and 3D printing technique. After preliminary tests, the sol-gel solution properties like viscosity, η, surface tension, γ and density ρ were optimized to obtain a sol-gel solution with jetting stability. The data clearly indicate that the degree of reaction of the solution at the time of coating application is a critical parameter for controlling jetting stability. Prehydrolysis prior to deposition is necessary to achieve desirable jetting properties. However, it is important to note that the reaction time of the sol-gel process before coating application (tr) was consistently set at 1 h.

The effects of roughness, chemical surface composition and the CA measurements suggest that the application of TZS (1 h) solution by 3D inkjet process leads to the obtainment of a surface with sub-micrometre level and micrometre features able to guarantee superhydrophobicity. But high adhesive force with water was measured (“Rose petal effect”). Decrease of adhesion force can be obtained after the application of fluorinated layer TZF(1 h).

On balance, these preliminary results shows that a novel sol-gel solution can be optimized to obtain, by a 3D printing approach based on micro-solenoid inkjet printing, surfaces with super or hydrophobic properties. It is believed that this simple and new 3D printing method presented here can expand the new application of superhydrophobic surface with highly and lower adhesive on several substrates for application in different fields.

Author contributions TR wrote the main manuscript. CM and TR prepared graphical abstract. All authors reviewed the manuscript.

Compliance with ethical standards

Conflict of interest The authors declare no competing interests.

References

1. Chen W, Fadeev AY, Hsieh MC, Oner D, Youngblood J, McCarty TJ (1999) Ultrahydrophobic and ultralyophobic surfaces: some comments and examples. Langmuir 15:3395–3399
2. Li XM, Reinhoudt D, Crego-Calama M (2007) What do we need for a superhydrophobic surface? A review on the recent progress in the preparation of superhydrophobic surfaces. Chem Soc Rev 36:1350–1368
3. Cassie BD, Cassie ABD, Baxter S (1944) Wettability of porous surfaces. Trans Faraday Soc 40:546–551
4. Moulinet S, Bartolo D (2007) Life and death of a fakir droplet: impalement transitions on superhydrophobic surfaces. Eur Phys J E 24:251–260
5. Manoharan K, Bhattacharya S (2019) Superhydrophobic surfaces review: functional application, fabrication techniques and limitations. J Micromanuf 2:59–78
6. Taurino R, Fabbri E, Messori M, Pilati F, Pospiech D, Synytska A (2008) Facile preparation of superhydrophobic coatings by sol–gel processes. J Colloid Int Sci 325:149–156
7. Nakajima A, Fujishima A, Hashimoto K, Watanabe T (1999) Preparation of transparent superhydrophobic boehmite and silica films by sublimation of aluminum acetylacetonate. Adv Mater 11:1365–1368
8. Nakajima A, Fujishima A, Hashimoto K, Watanabe T (1999) Preparation of transparent superhydrophobic boehmite and silica films by sublimation of aluminum acetylacetonate. Adv Mater 16:1365–1368
9. Hozumi A, Takai O (1997) Preparation of ultra water-repellent films by microwave plasma-enhanced CVD. Thin Solid Films 303:222–225
10. Ogawa K, Soga M, Takada Y, Nakayama I (1993) Development of a transparent and ultrahydrophobic glass plate. Jpn J Appl Phys 32:L614
11. Sas I, Gorga RE, Joines JA, Thoney KA (2012) Literature review on superhydrophobic self-cleaning surfaces produced by electrospinning. J Polym Sci B Polym Phys 50:824–845
12. Guo Z, Liu W, Su B (2011) Superhydrophobic surfaces: from natural to biomimetic to functional. J Colloid Interface Sci 353:335–355
13. Cannio M, Boccaccini DN, Taurino R, Riva V, Gualtieri ML, Tognetti M, Hanuskova M, Cicconi M, Fey T, Rosa M, Novaresio V, Petaccia P, Romagnoli M, Boccaccini AR (2019) Digital Printing of Glass-ceramic Glazes, Ceram. in Modern Tech. https://doi.org/10.29272/cmt.2019.0010

14. Cannio M, Mortalò C, Prestianni M, Andreola F, Deambrosis SM, Miorin E, Zin V, Boccaccini DN, Romagnoli M (2021) Manufacturing of BaCe0.65Zr0.20Y0.15O3-δ-Ce0.85Gd0.15O2-δ structures by micro-extrusion 3D-printing. Mater Lett. https://doi.org/10.1016/j.matlet.2020.128970
15. Wang X, Cai X, Guo Q, Zhang T, Kobe B, Yang J (2013) I3DP, a robust 3D printing approach enabling genetic post-printing surface modification. Chem Commun 49:10064–10066
16. Zhang Y, Yin M, Ouyang X, Zhang AP, Tam H (2020) 3D μ-printing of polytetrafluoroethylene microstructures: a route to superhydrophobic surfaces and devices Appl Mater Today https://doi.org/10.1016/j.apmt.2020.100580
17. Li Y, Mao H, Hu P, Hermes M, Lim H, Yoon J, Luhar M, Chen Y, Wu W (2019) Bioinspired functional surfaces enabled by multiscale stereolithography. Adv Mater Tech 4:1–7
18. Han S, Sung J, So H(2021) Simple fabrication of water harvesting surfaces using three-dimensional printing technology. Int J Precis Eng Manuf Green Tech 8:1449–1459
19. Orsi G, De Maria C, Montemurro F, Chauhan VM, Aylott JW, Vozzi G (2015) Combinig inkject printing and sol-gel chemistry for making pH-sensitive surfaces. Curr Top Med Chem 15:271–278
20. Gvishi R, Sokolov I (2020) 3D sol–gel printing and sol–gel bonding for fabrication of macro- and micro/nano-structured photonic devices. J Sol-Gel Sci Technol 95:635–648
21. Derby B (2010) Inkjet printing of functional and structural materials: fluid property requirements, feature stability and resolution. Annu Rev Mat Res 40:395–414
22. Butt MA (2022) Thin-film coating methods: a successful marriage of high-quality and cost-effectiveness—a brief exploration. Coatings 12:1115–1136
23. Jang D, Kim D, Moon J (2009) Influence of fluid physical properties on ink-jet printability. Langmuir 25:2629–2635
24. Bhushan, B., Nosonovsky, M. (2012). Rose Petal Effect. In: Bhushan, B. (eds) Encyclopedia of Nanotechnology. Springer, Dordrecht. https://doi.org/10.1007/978-90-481-9751-4_157
25. Rotenberg Y, Rajagopalan L, Neumann AW (1983) Determination of surface tension and contact angles from the shapes of axisymmetric fluid interfaces. J Colloid Interf Sci 93:169–183
26. Machekposhti SA, Movahed S, Narayan RJ (2020) Physicochemical parameters that underlie inkjet printing for medical applications. Biophysics Rev 1:011301
27. Taurino R, Fabbri E, Pospiech D, Synytska A, Messori M (2014) Preparation of scratch resistant superhydrophobic hybrid coatings by sol–gel process. Prog Org Coat 77:1635–1641
28. Messori M, Toselli M, Pilati F, Fabbri P, Pasquali L, Montecchi M, Nannarone S, Tonelli C (2005) Perfluoropolyether-based organic-inorganic hybrid coatigs: preparation and surface characterisation. Surf Coat Int Part B: Coat Trans 88:243–249
29. Zhang J, Yue P (2020) A level-set method for moving contact lines with contact angle hysteresis. J Comp Phys 418:109636–109657
30. Feng L, Zhang Y, Xi J, Zhu Y, Wang N, Xia F, Jiang L (2008) Petal effect: a superhydrophobic state with high adhesive force. Langmuir 24:4114–4119
31. Widom B (2004) Capillarity and wetting phenomena: drops, bubbles, pearls, waves. Phys Today 57:66–67
32. Herminghaus S (2000) Roughness-indiced non-wetting. Eur Lett 52:165–170
33. Gersh OB, Eli R (2009) Contact angles of nanodrops on chemically rough surfaces. Langmuir 25:9285–9289

Publisher's note Springer Nature remains neutral with regard to jurisdictional claims in published maps and institutional affiliations.

Springer Nature or its licensor (e.g. a society or other partner) holds exclusive rights to this article under a publishing agreement with the author(s) or other rightsholder(s); author self-archiving of the accepted manuscript version of this article is solely governed by the terms of such publishing agreement and applicable law.